Maximum Entropy Derived Statistics of Sound-Speed Structure in a Fine-Grained Sediment Inferred From Sparse Broadband Acoustic Measurements on the New England Continental Shelf

David P. Knobles ⓘ, Preston S. Wilson, John A. Goff, Lin Wan, Michael J. Buckingham, Jason D. Chaytor, and Mohsen Badiey

Abstract—Marginal probability distributions for parameters representing an effective sound-speed structure of a fine-grained sediment are inferred from a data ensemble maximum entropy method that utilizes a sparse spatially distributed set of received pressure time series resulting from multiple explosive sources in a shallow-water ocean environment possessing significant spatial variability of the seabed. A remote sensing seabed acoustics experiment undertaken in March 2017 off the New England Shelf was designed so that multiple independent analyses could infer the statistical properties of the seabed. The current analysis incorporates the measured horizontal variability from interpretations of a subbottom profiling survey of the experimental area. An idealized range- and azimuth-dependent parameterization of the seabed is derived from identification of *horizons* within the seabed that define multiple sediment layers. A sparse set of explosive charges were deployed on circular tracks with radii of about 2, 4, and 6.5 km with an acoustic array at the center to correlate a set of random measurements to physical acoustic processes that characterize the seabed. The mean values of a surface sound speed ratio and a linear sound speed gradient for the fine-grained sediment layer derived from 12 data samples processed in the 25–275-Hz band provide an estimate of the effective sound-speed structure in a 130-km^2 area. The inferred sediment sound speed values are evaluated by predicting measured time series data not used in the statistical inference, and are also compared to historical measurements. Finally, the low-frequency maximum entropy estimate of the sediment sound speed along with physical measurements derived from piston core measurements are utilized to estimate the sediment grain bulk modulus.

Index Terms—Maximum entropy, remote sensing, seabed acoustics.

I. INTRODUCTION

THE purpose of the Seabed Characterization Experiment (SBCEXP) 2017 was to infer via remote sensing the physical characteristics of a surface sediment layer composed of fine-grained materials in their natural or undisturbed marine state. This requires evaluating geoacoustic models and quantifying information content in the measurements and uncertainties in the inferences made on the seabed parameter values [1]–[16]. A complicating feature of the environment discussed in this study is the high level of spatial variability of the seabed layering that affects the coherent structure of the acoustic field. A central question for the statistical inverse problem as applied to SBC-EXP is how to interpret or create the *a priori* evidence or *state of knowledge* from preliminary and ongoing analyses of surveys of the experimental area made prior to the main acoustic experiment. The interpretation of the existing physical evidence on the seabed generally leads to the creation of an effective geoacoustic model, which reflects a potential to infer information about the parameters from the data samples collected in the experiment.

The focus of this paper is a subset of measurements inspired by the idea that an acoustic measurement made in a region possessing a high degree of seabed variability, such as those typically found in littoral ocean environments, can be viewed as a *random sample* from an ensemble, and that such experiments should be connected with the physical phenomena characterizing the interaction of sound with the ocean waveguide. It is within this framework of analysis that information content contained in the acoustic data about the seabed is quantified.

The experimental measurements were made in a 330-km^2 area known as the New England *Mudpatch* (see Fig. 1). The northern and southern boundaries are defined by east-west shipping lanes. The region was originally studied by Twichell who reported a *pond* of a fine-grained sediment with a maximum thickness of about 13 m [17]. In preparation for the main 2017 acoustic field experiment a high resolution bottom profiling survey was

D. P. Knobles is with Knobles Scientific and Analysis, Austin, TX 78755 USA (e-mail: dpknobles@kphysics.org).

P. S. Wilson is with the Department of Mechanical Engineering and Applied Research Laboratories, The University of Texas at Austin, Austin, TX 78713 USA (e-mail: pswilson@mail.utexas.edu).

J. A. Goff is with the Institute for Geophysics, University of Texas, Austin, TX 78713 USA (e-mail: goff@ig.utexas.edu).

L. Wan and M. Badiey are with the College of Engineering, University of Delaware, Newark, DE 19716 USA (e-mail: wan@udel.edu; badiey@udel.edu).

M. J. Buckingham is with the Marine Physical Laboratory, Scripps Institution of Oceanography, University of California, San Diego 9500 Gilman Drive La Jolla, CA 92093-0238 USA (e-mail: mjb@mpl.ucsd.edu).

J. D. Chaytor is with the U.S. Survey, Woods Hole, MA 02543 USA (e-mail: jchaytor@usgs.gov).
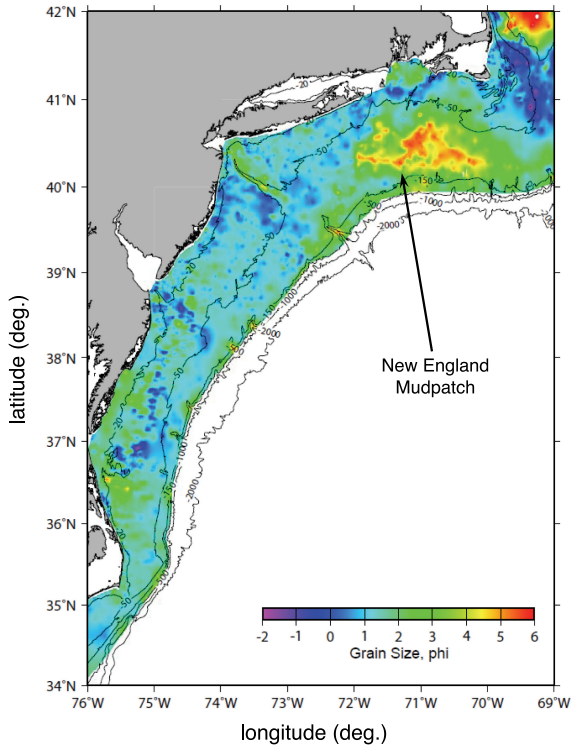
Fig. 1. New England Mudpatch. Northeast U.S. Shelf seafloor grain size Source: [18].
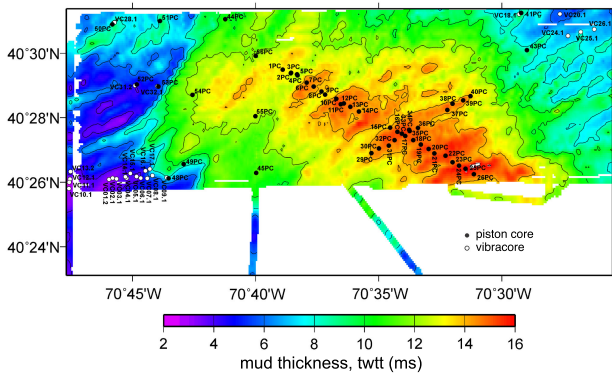

Fig. 2. Piston and vibracore locations and sediment two-way travel time for surface mud layer. Source: [18].
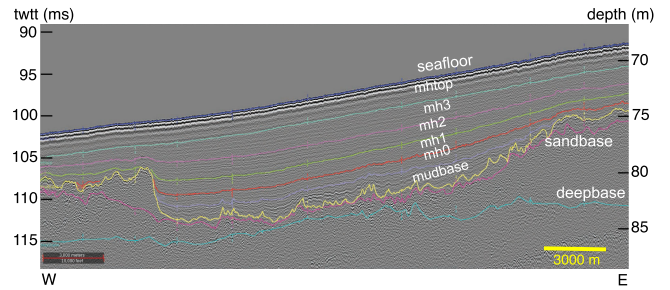

Fig. 3. Layering horizons along E-W bottom profiling survey line MP13. Source: [18].

from SW to NE. Approximately 4500 kg of sediment were extracted during two days of coring from *R/V Endeavor*.

Fig. 3 presents an example of seabed layering from the bottom profiling survey two-way travel times [18]. Several *horizons* are color coded for visualization purposes. The first sediment layer is the fine-grained sediment previously discussed by Twichell *et al.* [17]. The mud layer is interpreted to lie between the seafloor reflection and the high-amplitude mud base reflector. Within the mud unit, several internal reflectors (mh0 to mhtop) are traced, providing a stratigraphic history of the mud deposition. Below the mud base is a *thin* irregular horizon called the *sand base* (*sb*) followed by a *deep base* (*db*). Other deep base horizons were also identified. The layer beneath the fine-grained sediment was previously identified as a fine to medium sand in [17] from measured cores and also in the more recent PS survey [19] where some of the cores penetrated through the fine-grained sediment layer and into the sand sediment and also from direct measurements performed by Yang and Jackson during the main acoustic experiment [20].

The two-way travel time map of the surficial fine-grained sediment in Fig. 2 and the example of the range variability of the sediment layering in Fig. 3 demonstrate that the experimental area possesses significant horizontal variability in the thicknesses of the fine-grained sediment and the deeper sediment layers. However, one cannot ascertain from Fig. 2 if the variability of the two-way travel time includes variability of the sound speed within the volume of the surficial fine-grained sediment layer. An initial examination of the subbottom profiling survey data did not appear to yield specific information on the depth dependence of the sound speed within the fine-grained sediment. With regard to horizontal variability, Twichell *et al.* reported that the average grain size in the fine-grained sediment mixture generally increased from west to east across the *Mudpatch* [17]. It was hypothesized that for an acoustic experiment that covered a large enough spatial scale, it might be possible to correlate such a variability within the volume of the fine-grained sediment with the measured variability in the acoustic field.

Inspired by Jaynes' concept of connecting physics to random experiments [21], a sparse set of MK-64 signal underwater sound (SUS) explosive sources on circular tracks served as random experiments of sound propagation along different radials emanating from the intersection of the NW-SE and the NE-SW sediment channels where an acoustic array of hydrophones was positioned. The data ensemble maximum entropy method

performed in July 2015 [18]. Also, the U.S. Geological Survey (USGS) conducted a dense piston core (PS) survey of the experimental area in 2016 along planned propagation paths for the 2017 experiment [18]. The acoustic measurements were undertaken from late February to mid April of 2017, during which the water column possessed only small variability. The rationale was to mitigate the uncertainty of the water column in the general statistical inverse problem for seabed characterization.

Fig. 2 shows the PS positions superimposed onto a map of the two-way travel time inferred from the subbottom profiling survey. The sediment cores were collected on a main deposition channel that runs from NW to SE and also on another channel

[22]–[25] employed full waveform inverse techniques on the measured time series of multiple SUS events in the 25–275-Hz band to infer the statistics of the sound speed within the mud sediment over the central portion of the experimental area. The degree to which prior measurements are utilized in the quantification of information content plays a central theme in developing a seabed parameterization for statistical inference. The current analysis develops idealized sediment parameterizations made on the basis of the original Twitchell study [17], the 2015 subbottom profiling survey [18], a grain size analysis of the 2016 PSs [19], and direct sound speed measurements of the sediment below the base of the fine-grained sediment [20]. These parameterizations reflect an attempt to identify the simplest models supported by the acoustic data that accommodate the main physics of the interaction with a generally range and depth-dependent seabed. The idealized geoacoustic model based on the two-way travel time survey data consists of two sediment layers over a basement half-space, where the first and second layers are composed of a clay–sand–silt mixture and a fine sand, respectively. The range- and azimuth-dependent sediment thicknesses of the mixed fine-grained and the sand layers are constrained by the two-way travel time measurement.

It is demonstrated that a surface sound speed ratio and a sound speed gradient ambiguity can be partially resolved for the fine-grained sediment using a three-parameter model. The main conclusions from the current analysis is that the average sound speed ratio from all the data samples is on the order of 0.978. However, the sound speed gradient is large, with an average value of about 9.5 1/s. This *effective* gradient might be representative of a transition layer near the bottom of the fine-grained sediment where the sediment has an increased percent of medium sand. To within statistical significance one cannot detect variability of the ratio and the effective gradient over an 8-km spatial scale from west to east in the central area for the *Mudpatch*. Section II briefly discusses the experimental measurements. Section III describes the maximum entropy method as applied to the SUS time-series data. Section IV presents the results of the analyses and also utilizes physical parameter values derived from the PS measurements to estimate the grain bulk modulus of the fine-grained sediment. Section V provides a discussion and conclusion.

II. EXPERIMENTAL DESIGN

The design of an ocean geoacoustic experiment should reflect the planned methodology that will be used to analyze the data for their information content regarding the seabed structure. Here, we adopt Jaynes' concept that the design of a random experiment should be closely correlated with the physics of the phenomena being observed [21]. Fig. 4 shows the experimental design. Superimposed on the two-way travel time map for the fine-grained sediment are the positions of acoustic arrays and SUS MK-64 sources.

The design of the circular deployments was based in part on the assumption that each radial from the acoustic array at the center to a point on a circle of radius R represented a data sample drawn from the same but an unknown energy spectral
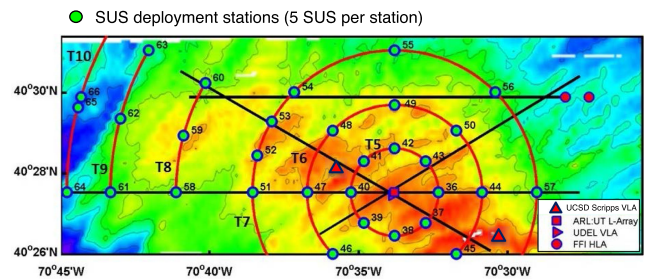

Fig. 4. Experimental design based on Jaynes' concept to quantify information content.

density (ESD) distribution of the mud sound speed. The idea adopted was that for a region *near* the center of the mud pond, a single ESD might be representative of the statistics of the sound speed because the water column deposition mechanics would be similar. Such an experimental design for a seabed acoustic experiment has been previously discussed in [26]–[28].

During March 17–18, 2017, five MK-64 SUS were hand-deployed at each SUS deployment station in 20-s intervals off the stern of the RV Neil Armstrong. The total number of successful deployments was 176. The nominal detonation depth was about 18.3 m. The method of deploying the MK-64 sources was convenient because a hand-held global positioning system recorded the deployment positions to within a few meters of accuracy.

III. STATISTICAL INFERENCE METHODOLOGY

This section discusses the details of the statistical remote sensing methodology used in the analysis of the SUS data for their information content on the properties of the fine-grained sediment. At the center is a statistical waveform inversion method. Waveform inversion methods have played an important role in remote sensing in shallow water environments [29]–[31].

A. Error Function

Connecting the physics of the seabed to N random SUS time-series measurements $((P_D)_n(t) : n = 1, 2, 3, \ldots, N - 1, N)$ starts with the concept of a cost or error function $E_n((P_M)(\theta, \tau_s), (P_D)_n)$, where $(P_M)(\theta, \tau_s)$ is a simulated time series that depends on an *effective model* representation M of the waveguide where the *hypothesis* vector θ contains a subset of these parameters that are viewed as random. The error function used in this study is the square error

$$E(P_M(\theta, \tau_s), P_D) = \frac{1}{2} \sum_k (P_D(t_k) - P_M(\theta, t_k + \tau_s(\theta)))^2 \tag{1}$$

where the sum is over the discrete time samples. This error function is consistent with a likelihood function whose functional form assumes that the statistics of the error function are Gaussian [8], [12]. The time shift $\tau_s(\theta)$ is determined for each hypothesis θ such that Ξ is minimized where

$$\Xi = 1 - \frac{1}{Q} \left| \int dt P_M(t) P_D(t + \tau_s) \right| \tag{2}$$

and

$$Q = \sqrt{\int dt P_M^2(t) \int dt P_D^2(t)} \tag{3}$$

such that $\tau_s(\theta)$ *aligns* the modeled and measured time series to a reference set of arrivals observed in both the measured and modeled time series. In the current study, the reference arrivals are the first 2–3 pressure peaks in the time series. In a sense this constraint on the error function is based on a *feature analysis* of the measurement. A feature constraint as used in this analysis refers to a part of a measurement that the model is required to fit.

In practice, P_M is a band-limited Fourier transform of the product of a Green's function satisfying the inhomogeneous wave equation for an idealized point source waveguide boundary conditions with the MK-64 source function $S(f)$ [32], [33]

$$P_M(r, \theta, t, t_s) = \int df G(r, \theta, f)) S(f) \exp(-2\pi i f(t + t_s)) \tag{4}$$

such as that provided by the finite difference range-dependent parabolic equation algorithm (RAM-PE) developed by Collins [34].

B. Maximum Entropy

Jaynes' maximum entropy method as applied to data ensembles [24], [25] provides a means to compute a conditional posterior probability distribution for each data sample, $P(H|P_D, M)$. In a Bayesian approach, the parameters in the hypothesis space are viewed as nondeterministic and thus random. Frequentist statistics are based on estimating θ and then using this estimate for all further predictions [35]. Frequentist methods assume that the true value $\hat{\theta}$ is fixed (deterministic) but unknown. In the frequentist perspective, the point estimate $\hat{\theta}_m$ is viewed as a random variable because a data set sample is also viewed as a random selection from a probability distribution. In a frequentist approach, a point estimate for θ, such as provided by $\hat{\theta}$, where $\hat{\theta} \in \theta$ such that $E(\hat{\theta}) \leq E(\theta)$ for all θ is nondeterministic since the data are random. However, individual point estimates cannot be assigned an uncertainty.

The goal of Bayesian reasoning is to infer from the measurements the conditional probability distributions $P(\theta_n|D_n, M)$. Employing the Kullback relative entropy functional [36]

$$S_n = \int d\theta P(\theta|D_n, M) \ln \frac{P(\theta|D_n, M)}{P(\theta, M)} \tag{5}$$

the conditional canonical probability distribution was previously derived [24]. The result is the canonical distribution [37]

$$P(\theta_n|D_n, M) = P(\theta_n, M) \frac{\exp[-\beta_n E_n(\theta_n, D_n)]}{Z_n} \tag{6}$$

where Z_n and β_n are analogous to the partition function and the Boltzmann factor, respectively, with

$$Z(\beta_n) = \int dH P(H, M) \exp[-\beta_n E_n(\theta_n, D_n)] \tag{7}$$

and where β_n is determined by solving the constraint integral equation

$$< E_n > = \int dH \frac{\exp[-\beta_n E(H, D_n)]}{Z_n(\beta_n)} E_n(\theta_n, D_n). \tag{8}$$

The new idea put forth in [24] was finding an estimate for the constraint $< E_n >$ so that β_n could be determined. Bilbro and Van den Bout [38] rewrote (8) as an integral over a continuous space of data samples D'

$$< E_n > = \int dD' P(D'|\hat{\theta}(D_n), M) E(\hat{\theta}(D_n), D')] \tag{9}$$

which was then estimated in [24] as

$$< E_n > \approx \frac{1}{K} \sum_j E(\hat{\theta}_n, D_j) \tag{10}$$

where $j = 1, 2, \ldots, K-1, K$.

The interpretation made in the data-ensemble maximum entropy concept is that β_n for a given inference using D_n, has contributions from all the random data samples, $D_1, D_2, \ldots, D_{N-1}, D_N$. From a statistical mechanics perspective β is the Boltzmann factor of $1/kT$ in $\exp(-\beta(E - E_0))$ where $E > E_0$ and E and E_0 represent energy states accessible to the system and the ground state, respectively. If one considers the analogy where E_0 is the inversion solution $E(\hat{\theta})$, an increase in β decreases the likelihood that there are solutions other than $\hat{\theta}$. Thus, for a given data sample, β is a measure of the uncertainty or in other words β is proportional to *information content* contained in P_D.

IV. GEOACOUSTIC MODEL AND PARAMETERIZATION

Initialization of an inverse problem requires addressing the *a priori* state of knowledge about the seabed, a suitable seabed model parameterization, and the definition of a data sample that can adequately support the selected model representation. Furthermore, a suitable model-data error function needs to be defined that can optimize information content. A governing guide in initializing the statistical inverse problem is the need for dimensional reduction of the parameter space, which is instrumental in avoiding over fitting the data with the model and thus mitigates the generalization error [35]. In this study, these goals are accomplished by utilizing the prior state of knowledge provided from the survey data [18]–[19], the literature, and sensitivity studies. Dimensional reduction then leads to the concept of an effective representation of the seabed; namely a representation that may have qualities that are not fully consistent with the *true* seabed structure.

This section discusses an idealized geoacoustic model of the seabed that may be suitable to provide useful information content about the physical properties of the fine-grained sediment from the acoustic measurements in the water column. The idea was to start with a best guess for a model representation that the measured data could support, and to then, using trial by error, make changes that had the potential to improve the consistency of information about the seabed that could be inferred from the statistical approach applied in the current work.

TABLE I
GEOACOUSTIC PARAMETERIZATION AND PROPOSED UPPER AND
LOWER BOUNDS

Parameter	units	lower bound	upper bound
$C_1(Z=0)$	$\frac{m}{s}$	1400	1485
g_1	$\frac{1}{s}$	0	20
$\rho_1(Z=0)$	g cm^{-3}	1.25	2.0
$\alpha_1(Z=0)$	$\frac{dB}{m}$ @ 1 kHz	0.01	0.01
ϵ_1		1.8	1.8
$C_2(Z=H_1)$	$\frac{m}{s}$	1630	1670
ρ_2	g cm^{-3}	1.8	1.8
α_2	$\frac{dB}{m}$ @ 1 kHz	0.32	0.32
ϵ_2		1.8	1.8
$C_B(Z=H_1+H_2)$	$\frac{m}{s}$	1700	1800
ρ_B	g cm^{-3}	2.0	2.0
α_B	$\frac{dB}{m}$ @ 1 kHz	0.15	0.15
ϵ_B		1.8	1.8

On the basis of the assiduous Twichell analysis and the more recent PS data by Chaytor [19], the fine-grained sediment in the *Mudpatch* may be characterized as a sediment that lies between a clayey silt and sand silt. From the PSs analyzed thus far in the central section of the *Mudpatch* the porosity in the first 2–3 m is about 61% and the density 1.6 g cm^{-3}. A notional geoacoustic model for the central portion of the *Mudpatch* is given in Table I. It consists of a layer of a fine-grained sediment defined by a surface sound speed C_{1T}, a linear sound speed gradient g_1, a constant density ρ_1, an attenuation α_{1t} at the top of the layer, an attenuation at the bottom of the layer α_{1b}, an attenuation exponent ϵ_1, and a sediment thickness H_1. Beneath the surface layer is a homogeneous layer of sand defined by C_2, ρ_2, α_2, ϵ_2, and H_2. Beneath this second sediment layer lies an infinite basement half-space defined by C_B, ρ_B, α_B and an attenuation exponent ϵ_B.

To first order, there are two aspects of the fine-grained sediment that we want to infer information; the sound speed at the surface of the sediment C_{1T} or equivalently the sound speed ratio R_1 and an effective linear gradient g_1. It is assumed that for a given propagation track between the source and the receiver, C_{1T} is independent of range. Furthermore, since no specific information has been provided as of the time of this study on the depth dependence of the sound speed in the fine-grained sediment, it is assumed to linearly increase with depth

$$C(z) = C_{1T} + g_1 z, \quad 0 \le z \le H_1 \tag{11}$$

with $g_1 > 0$. Thus, the bottom sound speed of the sediment is

$$C_{1B,r} = C_{1T} + g_1 H_1(r) . \tag{12}$$

This assumed linear increase of the sound speed is intended to *capture* the difference in sound speeds at the top and bottom of the fine-grained sediment without introducing additional parameters that could potentially provide a more physical depth dependence of the fine-grained sediment. From an information content perspective, seeking a higher level of information about

the details of the depth dependence may result in an overall decrease of inferred sound speed information about the sediment.

The attenuation $A(f)$ in all the layers has the functional form

$$A(f) = \alpha(f/1000)^\epsilon \tag{13}$$

where f is the frequency in hertz. To first order, density gradients have previously been shown not to be important in seabed reflection coefficient studies at the lower frequencies [39], and as such the densities in each of the layers are assumed constant. Generally the important physical effects on the reflection from the seabed are due to the density contrast between layer interfaces. One note of caution is that the transition from the fine-grained sediment layer to the fine to medium sand layer may not be well-represented by a simple layer interface adopted in this study. Previous studies have examined the effects of a density gradient for such a sediment [15].

The measured two-way travel time $\tau_{\text{layer}}(r, \zeta)$, where r and ζ are the source range and azimuth coordinates relative to a receiver, acts as a constraint for layer sediment thickness for hypothesis values of C_1, g_1, and C_2. The constraint relationships are

$$H_1(r) = 2\frac{C_{1T}}{\mu_1(r,\theta) - g_1} \tag{14}$$

$$\mu_1(r) = \frac{4000}{\tau_1(r,\theta)} \tag{15}$$

with C_{1T} and C_2 in meter per second and τ in millisecond.

$$H_2(r) = 2\frac{C_2}{\mu_2(r,\theta)} \tag{16}$$

$$\mu_2(r) = \frac{4000}{\tau_2(r,\theta)} \tag{17}$$

where τ_1 is the two-way travel time for the fine-grained sediment layer and τ_2 is the sum of the two way travel times for the two sand layers beneath the fine-grained sediment layer.

The parameter bounds of the fine-grained sediment layer were established from the literature and preinversion sensitivity studies. Buckingham compared a prediction of porosity versus sound speed ratio (R) using his grain-shearing seabed acoustic theory to measured data [40]. For a porosity of 60%, the lowest R value is 0.950 and the highest is about 1.01. For the measured bottom water sound speed of 1469.5 m/s, this gives upper and lower bounds of about 1400 and 1485 m/s for the surface sound speed, respectively. Typical sound speed gradients for soft deep sea sediments are about 1.8 1/s [41]-[42]. However, preliminary modeling of the measured waveform strongly suggested higher sound speeds at the base of the fine-grained sediment caused by a rapid increase of the sound speed with depth. In an attempt to capture the possible existence of higher sound speeds in the fine-grained sediment the lower and upper bounds for the sound speed depth gradient were placed at 0 and 20 1/s, respectively. For a sediment composed primarily of clay a corresponding density is about 1.25 g cm^{-3}, whereas for a high sand content the density could be as high as about 2.0 g cm^{-3}. Thus, the lower and upper bounds of the fine-grained sediment density were selected as 1.25 and 2.0 g cm^{-3}, respectively.

The bounds of the sound speed in the sand layer C_2 were determined from the measurements made by Yang and Jackson [20] using an *in situ* measurement device that operated in the 2–10-kHz band. The mean value of the sound speed for the sand was 1650 m/s with a standard deviation of 20 m/s; hence the assumed lower and upper bounds of 1630 and 1670 m/s. The mean value corresponds to a fine sand classification. These sound speeds are consistent with the grain size measurements made by Chaytor [19], who determined from an assembly of 81 samples from the sand layer an average value of the grain size of 2.055 ϕ or 0.256 mm which corresponds to a fine sand classification. The assumed density for the sand is that of a fine sand. The inference of the attenuation and the attenuation frequency exponent have long been a subject in remote sensing of the geoacoustic structure in littoral ocean environments [25], [43]–[54]. The assumed sand attenuation and attenuation exponent values are those previously reported by Zhou *et al.* for an effective geoacoustic model for a fine-sand sediment [51].

V. RESULTS

The results of the application of the data-ensemble maximum entropy approach to analyze the SUS data are now presented. Two cases are shown, first, the five-parameter model that utilizes six SUS time series samples over a 0.40-s time window on the 2-km circle and second, a three-parameter model that utilizes six SUS time series samples over a 100- and 130-ms time window for the 2 and 4-km data samples, respectively. The bandwidth of the modeled and measured time series is approximately 25.1 to 275.2 Hz. Then, for each hypothesis point in the parameter space, the modeled transfer function is computed for 320 frequencies and is then convolved with the semiempirical SUS source function to produce the modeled pressure time series. For the six 2-km data samples and the six 4-km data samples, the parameter hypothesis space is sampled until convergence of the marginal distributions was obtained. Here, convergence refers to adding more samples in the multidimensional integrations and observing that the marginal distributions remain qualitatively unchanged. In the three-parameter model, this took about 15 000 samples. For the five-parameter model about 25 000 samples were required. Computations were made on two four-processor machines with 32- and 64-GB RAM, respectively. Run times on a single processor were about five days to compute 15 000 samples of the parameter space for an SUS data sample on the 2-km circle. Since the run time for RAM-PE is proportional to range, the run times for the 4-km case was about ten days. The Pade$'$ coefficient for RAM-PE was set to three.

The decision for the 25–275-Hz processing band and the limit to doing inversions only out to the 4-km circle was made in part to mitigate a large amount of electronic noise present on the L-array that became increasingly problematic with increasing source–receiver range. Still there exists a noisy portion of the signal approximately between 210 and 230 Hz. It appears that this was not a significant issue for the inversions presented in this study. With that said, the presence of noise generally degrades an inversion result and can cause generalization errors when methods to protect against over fitting are not implemented.
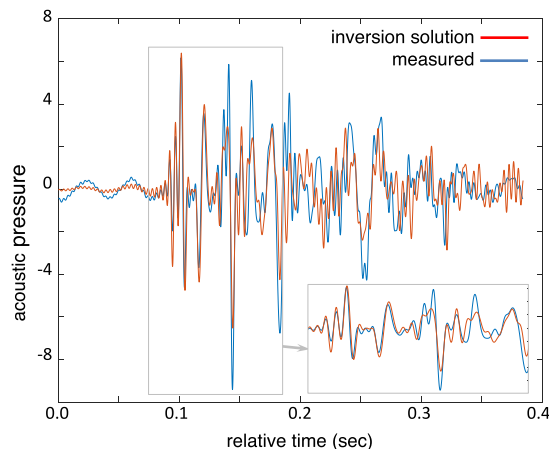

Fig. 5.   Comparison of measured time series for SUS station 37 with modeled using five-parameter inversion solution. Inset shows expanded time scale.

A. Five-Parameter Model

Fig. 5 shows a typical comparison of the measured pressure time-series data that results from a deployment of an SUS explosive charge on the 2-km circle to a modeled time series that uses an inversion solution. For SUS 37 the inversion solution is (C_{1T} = 1432.1 m/s, g_1 = 9.26 1/s, C_2 = 1653.3 m/s, ρ_1 = 1.76 g cm^{-3}, and C_3 = 1868.7 m/s). The source–receiver range for SUS 37 is 2.036 km. The enlarged portion is approximately the time window that includes arrivals mainly composed of that portion of the acoustic field that is confined to the water-column and the fine-grained sediment. The first two peaks in time series were present for all the data for both the 2- and 4-km samples. The cross correlation over the time window of these two arrivals [see (2) and (3)] was used to infer τ_s for each point sampled in the five-parameter hypothesis space of $E(P_M(\theta, \tau_s), P_D)$. The higher order modes (vertical angles) become increasingly sensitive to the sound-speed structure of the sand layers and half-space. For example, the large low-frequency Airy phase arrival is especially sensitive to the thickness of the sand and the basement sound speed. The Airy phase was recently discussed by Wan *et al.* for long-range SUS deployments made during the *Mudpatch* experiment [55].

The comparison in Fig. 5 suggests that the source levels, with which the modeled transfer function is convolved, are too low, but not low enough for the error function to be sensitive to physical parameters that affect the coherent multipath arrival structure. However, one might expect that errors in the assumed source level could bias inference of such parameters as the density and the attenuation. Table II provides the error matrix $E(\hat{\theta}_n, D_j)$. The diagonal elements correspond to the cost value at the inversion solution for each of the data samples.

The components that define the rows of the error function matrix are averaged to compute $< E >$ for each data sample [see (10)], which in turn allows for β to be computed via (8). Evaluating the multidimensional integrals in (5) and (6) then provide the conditional posterior distribution from which the marginal probability distributions are obtained via numerical quadrature over the *dummy* variables.

TABLE II
$E(\hat{\theta}_n, D_j)$ (X 10^{19}) FOR SUS DATA SAMPLES WITH 0.4-s TIME WINDOW ON 2-km CIRCLE FOR FIVE-PARAMETER REPRESENTATION OF THE SEABED

Data sample n	37	39	40	41	42	43
37	2.58	2.93	3.50	3.30	2.76	2.98
39	3.60	3.33	3.90	4.22	3.59	3.55
40	3.38	4.40	2.93	3.66	3.94	4.49
41	3.94	4.59	3.66	3.22	4.44	4.25
42	3.04	3.18	3.70	3.51	2.93	3.22
43	3.72	3.27	4.20	4.63	3.50	3.10

TABLE III
$E(\hat{\theta}_n, D_j)$ (X 10^{18}) FOR SUS DATA SAMPLES ON 2-km CIRCLE

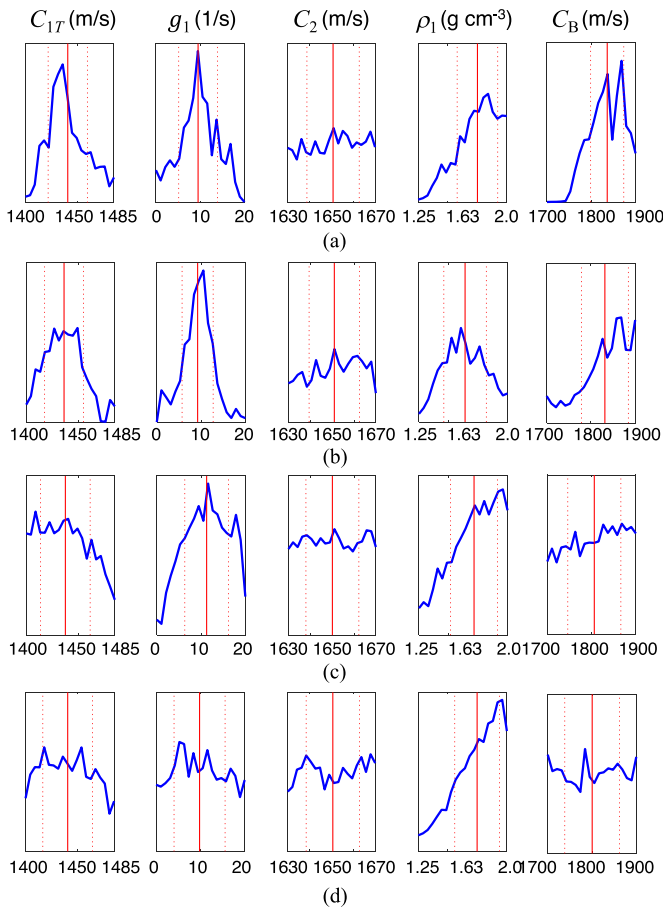| Data sample n	37	39	40	41	42	43
37	0.265	0.624	1.18	1.48	0.547	0.540
39	10.0	6.64	12.17	11.54	7.90	6.76
40	6.73	6.80	3.88	4.83	5.89	5.37
41	6.68	8.30	5.11	4.49	5.60	6.31
42	5.77	5.74	7.90	8.26	5.08	5.59
43	7.84	7.20	8.06	7.60	7.10	6.79

Fig. 6. Marginal distributions for SUS stations (a) 42, (b) 39, (c) 40, and (d) 41.

Fig. 6 displays examples of marginal probability distributions for the five-parameter model using the 2-km acoustic data. The distributions for C_2 were generally *flat* due in part to the assumed narrow bounds based on the reported measurements made on the sand by Yang and Jackson [20] and Chaytor [19]. The solid red lines on the marginal distributions denote the average values $< X >$ of the parameter X of the distributions and the dotted lines denote the values $< X > \pm \sigma_X$ where σ_X is the standard deviation. The data samples derived from the SUS 39 and SUS 42 events are examples where C_{1T} and g_1 are *well-resolved* in that symmetrical peaks in the marginals are observed, whereas data samples derived from the SUS 41 and SUS 40 events

are examples where C_{1T} and g_1 are *poorly resolved* in that symmetrical peaks in the marginals are not observed and the distributions are generally wide. The marginals for SUS 43 and SUS 37 events (not shown here) are similar to SUS 41 and SUS 40 in that the information content on the physical parameter values for the fine-grained sediment is low.

B. Inference Using three-Parameter Model in 0.1-s Time Window

During the course of the statistical inference analysis, it was discovered that the time-series arrival structure in a 100-ms time window for the 2-km data samples (see Fig. 5) and a 130-ms time window for the 4-km data samples was sensitive to both the sound-speed structure of the water column and the fine-grained sediment layer, and that the sensitivity rapidly decreased for parameters characterizing the sand and basement. This suggested that by carefully choosing the time window of the data samples one could mitigate the ambiguity between the fine-grained and the sand and basement parameters evident in the marginal distributions in Fig. 6.

Furthermore, while the *mean average* of ρ_1 from all six distributions is about 1.68 g cm^{-3}, which agrees with the value of 1.6 g cm^{-3} from the PSs, the majority of the ρ_1 marginal distributions are not symmetric with the peak values occurring near the upper boundary of 2.0 g cm^{-3}. In such cases, one should exercise caution in the interpretation of the statistics as generally $< \rho_1 >$ is less than the peak values of the marginals.

On the basis of the observation about the sensitivity of the time series in the 100- and 135-ms time window for the marginal distributions for ρ_1, it was hypothesized that an increased amount of information with minimal bias for C_{1T} and g_1 could be achieved with *dimensional reduction* [35] whereby the error function is summed only over the 100-ms and 135-ms time window arrivals, and ρ_1 is held fixed at its experimental value of 1.6 g cm^{-3}. The value of C_B is also held fixed (1800 m/s) since, as previously discussed, its affect on the mode 1 arrival structure is negligible. Thus, the three-parameter model consists of the parameters of C_{1T}, g_1, and C_2.

Tables III and IV provide the error matrix $E(\hat{\theta}_n, D_j)$ for the three-parameter model for the data samples on the 2- and 4-km circles, respectively. The same numerical steps as discussed in Section V-A are employed here to compute the marginal probability distributions.

TABLE IV

$E(\hat{\theta}_n, D_j)$ (x 10^{16}) FOR SUS DATA SAMPLES ON 4-km CIRCLE

Data sample n	44	45	47	48	49	50
44	4.79	5.97	5.09	5.56	6.36	7.25
45	3.77	2.45	4.24	2.60	3.67	5.53
47	4.30	6.10	4.056	5.58	6.51	4.60
48	6.63	6.54	7.00	5.9	6.52	8.59
49	6.80	6.61	7.59	6.35	5.55	9.84
50	6.00	9.66	6.90	7.31	4.44	3.65
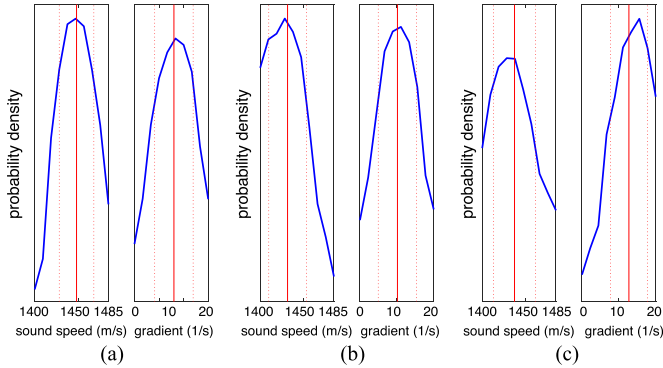
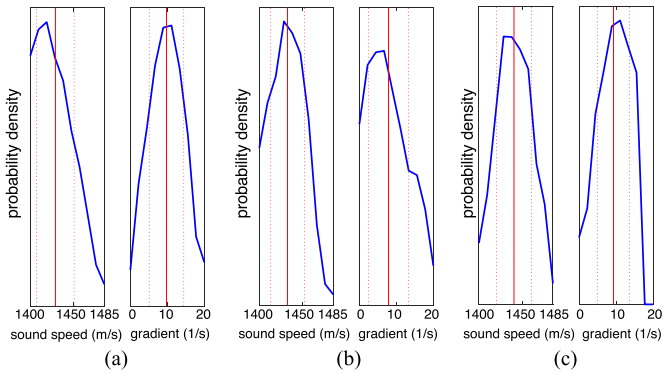Fig. 7. Marginals for SUS stations (a) 42, (b) 39, and (c) 40.

Fig. 8. Marginals for SUS stations (a) 44, (b) 47, and (c) 49.

Figs. 7 and 8 show examples of the marginals for C_{1T} and g_1 for data samples on the 2- and 4-km circles, respectively, and Tables V and VI present the statistics. While not all the marginal distributions are perfectly symmetric, it was observed that in most cases the average values were generally close to the peak values for both C_{1T} and g_1. For example, the largest difference of $\Delta_X = |\text{max of } P(X) - <X>|$ for all the data samples on the 2- and 4-km circles is about 5 m/s for C_{1T} and 1 1/s for g_1. Both of these largest differences are much less than the standard deviation for the parameter values.

Fig. 9 summarizes the main results of the analysis. It shows an average and a standard deviation of $C_{1T}/1469.5$ and g_1 inferred from 12 data samples corresponding to the deployment of the SUS on the circles of 2- and 4-km radius.

TABLE V

$<E>$, β, AND AVERAGE AND STANDARD DEVIATIONS FOR THREE-PARAMETER MODEL FOR DATA SAMPLES WITH 100-ms TIME WINDOW ON 2-km CIRCLE

Data sample	$<E>$	β	$<C_{1T}>$	$<g_1>$	$\sigma_{C_{1T}}$	σ_{g_1}
37	7.73x10^{17}	1.80x10^{-17}	1442.3	9.4	18.3	3.8
39	9.17x10^{18}	1.40x10^{-17}	1432.3	10.08	20.4	5.0
40	5.58x10^{18}	0.30x10^{-17}	1437.2	12.60	22.8	4.8
41	6.08x10^{18}	0.55x10^{-17}	1436.7	12.6	20.8	4.8
42	6.89x10^{18}	0.53x10^{-17}	1448.7	7.9	19.0	3.6
43	7.43x10^{18}	1.79x10^{-17}	1437.2	10.9	20.4	4.1

TABLE VI

$<E>$, β, AND AVERAGE AND STANDARD DEVIATIONS FOR THREE-PARAMETER MODEL FOR DATA SAMPLES WITH 130-ms TIME WINDOW ON 4-km CIRCLE

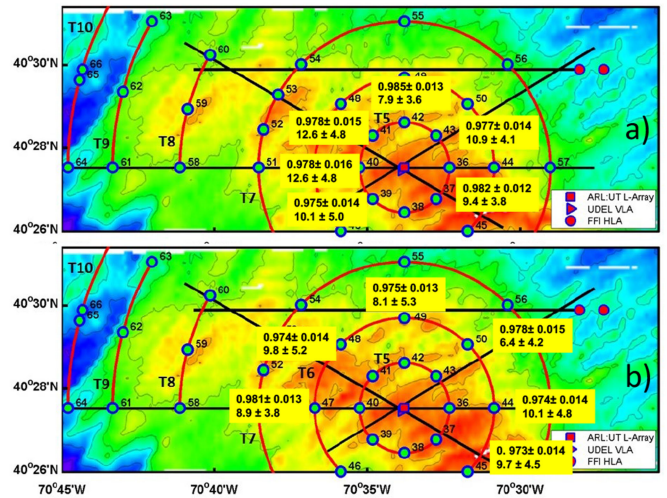| Data sample	$<E>$	β	$<C_{1T}>$	$<g_1>$	$\sigma_{C_{1T}}$	σ_{g_1}
44	5.84x10^{18}	5.0x10^{-18}	1433.1	10.1	19.2	4.8
45	3.71x10^{18}	6.14x10^{-18}	1428.3	9.7	20.1	4.5
47	5.26x10^{18}	5.3x10^{-18}	1440.8	8.9	19.5	3.8
48	6.87x10^{18}	5.90x10^{-18}	1431.3	9.8	20.2	5.2
49	7.12x10^{18}	3.37x10^{-18}	1433.0	8.1	18.8	5.3
50	6.32x10^{18}	1.88x10^{-18}	1435.4	6.4	21.5	4.2

Fig. 9. Summary of averages and standard deviations for sound speed ratio and sound speed gradient of fine-grained sediment for data samples on (a) 2-km and (b) 4-km circles.

For all 12 data samples on both the 2- and 4-km circles, the spread of the average sound speed ratios is 0.973 to 0.985 and the spread of the average sound speed gradients is 6.4 to 12.6 1/s. For all 12 data samples on both the 2- and 4-km circles, the spread of the standard deviations of the sound speed ratios is 0.012 to 0.016 and the spread of the standard deviations of the sound speed gradients is 3.6 to 5.3 1/s. From Fig. 9, an approximate point estimate for the sound speed ratio and sound speed gradient over the central area of the *Mudpatch* are the mean values of
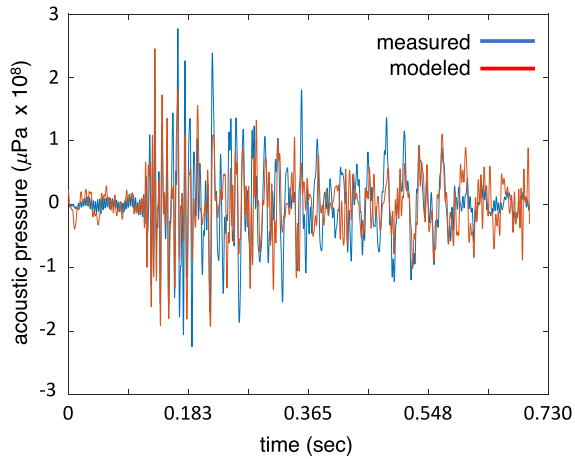
Fig. 10. Comparison of measured time series for SUS station 54 with modeled using maximum entropy determined values.
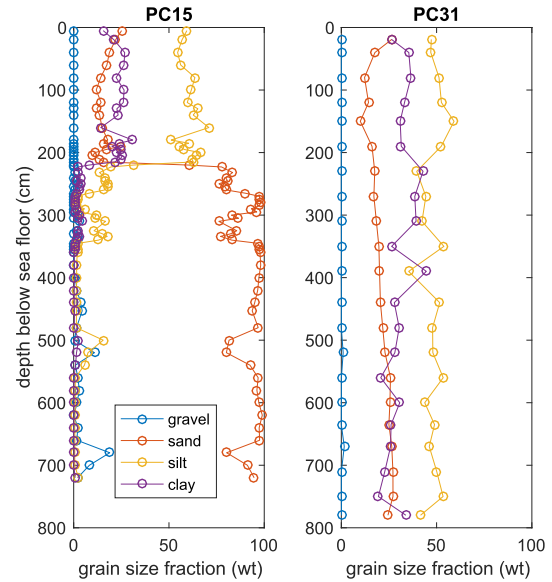

Fig. 11. Grain size fractions by weight for gravel, sand, silt, and clay are shown versus the depth beneath seafloor for PSs 15 and 31. PC31 is a typical core for the experimental site, whereas PC15 shows a sharp increase in sand content below 200 cm.

the average values, 0.9775 and 9.5 1/s, respectively. Using the measured bottom water sound speed of 1469.5 m/s, the point estimate for C_{1T} is 1436.4 m/s. Also, the two-way travel time of the fine-grained sediment at the central array is 15.2 ms, and from (14) and (15), $H_1(r = 0) = 11.3$ m.

Fig. 10 shows a model-data comparison of the pressure time series for the SUS 54 event, which lies on the 6.5-km circle. The model inputs are the mean values of the three-layer model established from the maximum entropy analysis of the SUS data samples on the 2- and 4-km circles. There is qualitative agreement, which shows the ability of the model to correctly predict the coherent multipath structure and the increase in the time spread of the signal that results from modal dispersion.

C. Comparison to Historical Measurements and Estimate of Grain Bulk Modulus

It is desirable to compare the maximum entropy point estimate of the sound speed ratio value of 0.9775 determined in the 25–275-Hz band (center frequency of 125 Hz) to historical data and to also infer the grain bulk modulus. To this end, several of the PC collected within the circular SUS transects were analyzed for grain size and porosity. PSs 9, 14, 15, 17, 19, 21, 26, 29, 33, 36, 38, and 40 were analyzed for porosity and PSs 9, 15, 21, 24, 31, 33, 36, 38, and 40 were analyzed for grain size. See Fig. 2 for the core locations. These cores indicate that the sediment in the center of the mudpatch consists of silt, clay, and sand with both horizontal and vertical spatial variability. Silt is typically the dominant constituent but sand can become dominant as depth increases. An extreme case of the latter is shown in Fig. 11, where PC15 (collected near the center of the SUS transect circles) exhibited a sharp transition to primarily sand at 200 cm below the seafloor (bsf). A more typical example for the center of the mudpatch is PC31, also shown in Fig. 11, collected about 1 km south of PC15, where silt represents about 50% of the sediment by weight at all depths. Clay is the next most-dominant constituent in the upper layers, at about 30% by weight, but the relative proportion of clay decreases with depth
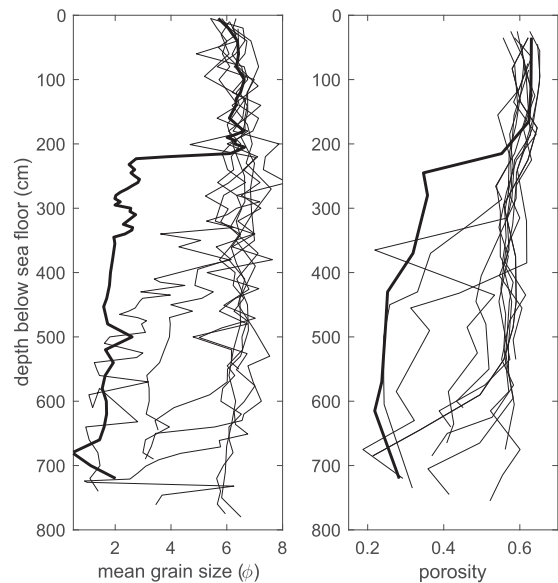

Fig. 12. Mean grain size (left) and porosity (right) versus depth for all cores is shown. The thicker curves are for PC15, illustrating how the sharp increase in sand content below 200 cm is expressed as a sharp increase in mean grain size (a decrease in ϕ) and a somewhat less sharp decrease in porosity. The sediment properties are more uniform across all cores above 200 cm bsf with variability increasing with depth.

while the relative proportion of sand increases. Gravel-sized particles typically represented less than 1% by weight in all cores.

Mean grain size and porosity for these cores is shown in Fig. 12. The effect of the increased sand content below 200 cm in PC15 (thicker curves) can be seen as sharp decreases in ϕ and porosity. These results indicate that the upper 200 cm is more
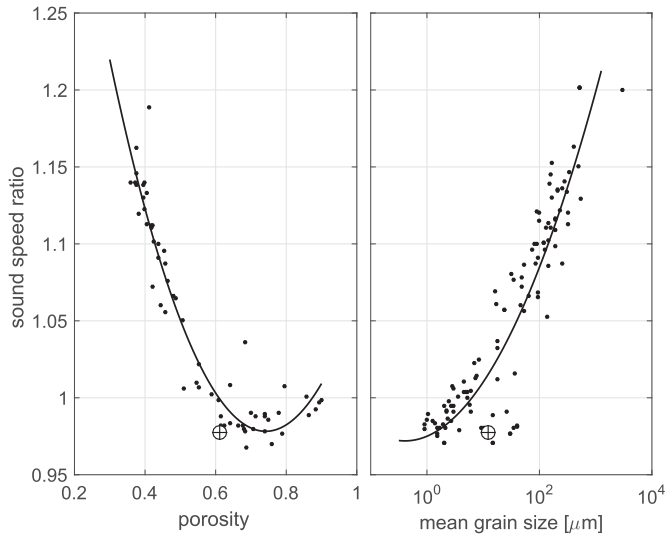
Fig. 13.   Dependence of sound speed ratio on porosity and mean grain size is shown. Historical data collected by Buckingham (2005) is shown with solid black circles. The solid lines are polynomial fits to the data. The present average of upper layer sound speed inferences within the center of the mudpatch (a sound speed ratio of 0.9775) is shown with the $\oplus$ symbols at the mean porosity and mean grain size observed within the upper 200 cm of the PSs. Figure adapted from Ref. [56].

uniform, while spatial variability increases as depth increases. The mean grain size averaged across these cores between 0 and 200 cm bsf is 6.33ϕ, which is equivalent to 12.4 μ m diameter. The standard deviation of the core mean grain diameter was 2.0 μm. The mean porosity averaged across these cores between 0 and 200 cm bsf was 0.612 with a standard deviation of 0.02. These mean grain parameters were used to compare the global inferred sound speed ratio (0.9775) to historical sound speed measurements in Fig. 13. The sound speed data shown in Fig. 13 is that collected in [56, Figs. 8 and 10]. The solid lines are polynomial best-fit curves to the data. The results of the present work are shown with the $\oplus$ symbols, and they are generally consistent with the historical data, but fall near the lower sound speed limit of the historical data, and below the best-fit curves. It is important to note that since the historical data were obtained at higher frequencies as compared to the current inference result, one might ascribe the generally lower sound speed value to a frequency dispersion mechanism such as that predicted by the viscous grain shearing model [57].

We utilized the aforementioned measured physical properties of the PS measurements made by Chaytor [19] to estimate the sediment bulk grain modulus. To this end we identified the ME point estimate as the Wood/Mallock sound speed c_0 from Wood's equation [58], [59], which is the low-frequency limit of the sediment sound speed. A note of caution is that since the mud surface sound speed estimate was made using acoustic data in the 25–275-Hz band this sound speed assignment is only an approximation and can thus lead to a bias in estimating the bulk grain modulus. The Wood/Mallock sound speed is

$$c_0 = \sqrt{\frac{K_0}{\rho_0}} \qquad (18)$$

where

$$\frac{1}{(K_0)} = \frac{N}{(K_w)} + \frac{(1 - N)}{(K_g)} \qquad (19)$$

and

$$\rho_0 = N\rho_w + (1 - N)\rho_g \qquad (20)$$

where N, ρ_w, ρ_g, K_w, K_g are the sediment porosity, the density of seawater, the sediment grain density, the seawater bulk modulus, and the sediment grain bulk modulus. The average value of N, ρ_0, and the grain size in the central region of the *Mudpatch* are 0.612, 1600 kg/m^3, and 6.33ϕ (12.4 μ m diameter), respectively. The value of ρ_0 is the same value used for ρ_1 in Section V-B; namely it is the experimental value of the mud density. It is assumed that the pore fluid is seawater with $\rho_w = 1030\,\text{kg/m}^3$ and $K_w = 2.2242\,\text{GPa}$. Solving for ρ_g in (20) gives $\rho_g = 2499.1$ kg/m^3. Then, (18) gives $K_0 = 3.3014$ GPa. From (19), K_g is approximately 13.98 GPa, which is characteristic of kaolinite.

VI. DISCUSSION AND CONCLUSION

In March–April 2017, acoustic remote sensing measurements were made in an area called the New England *Mudpatch* for the purpose of inferring the physical properties of a fine-grained sediment with a large degree of horizontal variability over a 360-km^2 area. This paper focused on an analysis of a portion of the acoustic data generated by the deployment of SUS MK-64 explosive sources on two circular tracks of 2 and 4 km with an acoustic array at the center. A maximum entropy method utilized full waveform inversion of the received pressure time series from multiple data samples to infer the marginal probability distributions for the surface sound speed and a sound speed depth gradient of the fine-grained sediment. The sampling of the range and azimuth-dependent layer sediment thicknesses were constrained with a two-way travel time survey of the experimental area that related sediment thickness to sound speed in the various layers. The range-dependence along each propagation path was adequately addressed with a finite element PE equation methodology. The application of the maximum entropy method to 12 SUS data samples resulted in a point estimate of the sound speed ratio of the fine grained sediment of about 0.9775 or a surface sound speed prediction of about 1436.4 m/s. The solution was also characterized by a large sound speed gradient, about 9.5 1/s. The USGS PS measurements were combined with the ME estimate of the sound speed that provided the estimate of 13.981 GPa for the grain bulk modulus, which is characteristic of kaolinite.

The characterization of the fine-grained sediment in the New England *Mudpatch* appears significantly more complicated than thick sediments. It possesses a high degree of spatial variability that motivated the use of an effective geoacoustic model. The effective sound speed gradient in the mud layer remains may be the most perplexing characteristic in the SUS analyses. The large gradients were clearly much higher than what one might expect from deep sea thick mud sediments [41], [42] and from other shallow water areas where the mud was known to have a significant thickness. In such cases the expected gradients are

1–2 1/s. An early preinversion observation was that if one did not assume a linear gradient, then the inferred sound speed ratio was around unity. There is a natural ambiguity between surface sound speed and the gradient. But, as was found the gradients appeared to have a limit as to its size, and distributions were found for sound speed and gradient parameter values.

Because inversion solutions are by definition an effective geoacoustic profile, it is possible that the sound speed gradient does not have a physical basis. However, it is useful to try and attempt to see if there is a correlation between an effective parameter value and a physical description of the sediment. At the risk of some speculation, possible insight into the inferred sound-speed structure comes from some of the analysis on PSs, suggesting that there is a 2–3-m transition interval above the mud base that is a combination of silt and clay and medium-coarse size quartz where the concentration of the sand increases rapidly with increasing depth in the interval. This transition interval is not of a fixed thickness and can be anything from absent to several meters in thickness, depending on the location. Shells and shell fragments of various sizes are present through this interval. Below this is medium-coarse sand that varies in composition between 75% and 90%. Goff *et al.* [18] also provide some evidence of the existence of a transition layer 2–3-m above the mud base from an impedance analysis of the horizons within the mud layer. A preliminary geological interpretation of the apparent increase of acoustic impedance above the interface of the fine-grained sediment and the sand interface is that due to a dynamic sand base with a forcing function provided by storms, the initial deposition of the Holocene fine-grained sediment was mixed with coarser grain-size sands. This mixing occurred over a time span during which about 2–3-m of sediment was deposited. The dynamics of the sand decreased and the sand mixture subsided, thus allowing the remainder of the fine-grained sediment (about 8 m) to be deposited in a normal manner. Still, the issue of the large effective gradient is an open scientific question.

REFERENCES

[1] S. D. Rajan, J. F. Lynch, and G. V. Frisk, "Perturbative inversion methods for obtaining bottom geoacoustic parameters in shallow water," *J. Acoust. Soc. Amer.*, vol. 82, pp. 998–1017, 1987.

[2] J. X Zhou, X. Z. Zhang. P. H. Rogers, and J. Jarzynski, "Geoacoustic parameters in a stratified sea bottom from shallow water acoustic propagation," *J. Acoust. Soc Amer.*, vol. 82, pp. 2068–2074, 1987.

[3] M. D. Collins, W. A. Kuperman, and H. Schmidt, "Nonlinear inversion for ocean-bottom properties," *J. Acoust. Soc. Amer.*, vol. 92, pp. 2770–2783, 1992.

[4] S. E. Dosso, M. L. Yeremey, J. M. Ozard, and N. R. Chapman, "Estimation of ocean-bottom properties by matched field inversions of acoustic field data," *IEEE J. Ocean. Eng.*, vol. 18, no. 3, pp. 232–239, Jul. 1993.

[5] H. Schmidt and A. Baggeroer, "Physics-imposed resolution and robustness issues in seismo acoustic parameter inversion," in *Full Field Inversion Methods in Ocean and Seismo-Acoustics*, O. Diaschok *et al.*, Eds. Dordrecht, The Netherlands: Kluwer, 1995, pp. 85–90.

[6] A. Thode, M. Zanolin, E. Naftali, I. Ingram, P. Ratilal, and N. Makris, "Necessary conditions for a maximum likelihood estimate to become asymptotically unbiased and attain the Cramer-Rao lower bound. II. Range and depth localization of a sound source in an ocean waveguide," *J. Acoust. Soc. Amer.*, vol. 112, pp. 1890–1910, 2002.

[7] N. C. Makris, "Parameter resolution bounds that depend on sample size," *J. Acoust. Soc. Amer.*, vol. 99, pp. 2851–2861, 1996.

[8] M. K. Sen and P. L. Stoffa, "Bayesian inference, Gibbs' sampler and uncertainty estimation in geophysical inversion," *J. Geophys. Prospecting*, vol. 44, pp. 313–350, 1996.

[9] M. Badiey, A. H.-D. Chaeng, and Y. Mu, "From geology to geoacoustics-evaluation of Biot-Stoll sound speed and attenuation for shallow water acoustics," *J. Acoust. Soc. Amer.*, vol. 103, pp. 309–320, 1998.

[10] S. D. Rajan, J. A. Doutt, and W. M. Carey, "Inversion for the compressional wave speed profile of the bottom from synthetic aperture experiments conducted in the hudson canyon area," *IEEE J. Ocean. Eng.*, vol. 23, no. 3, pp. 174–187, Jul. 1998.

[11] S. E. Dosso and M. J. Wilmut, "Quantifying data information content in geoacoustic inversions," *IEEE J. Ocean. Eng.*, vol. 27, no. 2, pp. 296–304, Apr. 2002.

[12] S. E. Dosso, "Quantifying uncertainty in geoacoustic inversion. I. A. fast Gibbs sampler approach," *J. Acoust. Soc. Amer.*, vol. 111, pp. 129–142, 2002.

[13] M. Zanolin, I. Ingram, A. Thode, and N. C. Makris, "Asymptotic accuracy of geoacoustic inversions," *J. Acoust. Soc. Amer.*, vol. 116, pp. 2031–2042, 2004.

[14] M. D. Richardson and K. B. Briggs, "Empirical predictions of seafloor properties based on remotely measured sediment impedance," in *High Frequency Ocean Acoustics*, M. Porter, M. Siderius, and W. A. Kuperman, Eds. College Park, MD, USA: Amer. Inst. Phys., 2004.

[15] C. Holland, "Remote sensing of sediment density and velocity gradients in the transition layer," *J. Acoust. Soc. Amer.*, vol. 118, pp. 163–177, 2005.

[16] P. H. Rogers, J. X Zhou, X. Z. Zhang, and F. Li, "Seabottom acoustic parameters from inversion of yellow sea experimental data," in *Experimental Acoustic Inversion Methods for Exploration of the Seabed*, A. Caiti, J.-P. Hermand, and S. Jesus, Eds. Berlin, Germany: Springer, 2012.

[17] D. C. Twichell, C. E. McClennen, and B. Butman, "Morphology and process associated with the accumulation of the fine-grained sediment deposit on the southern New England Shelf," *J. Sedimentary Petrology*, vol. 51, pp. 269–280, 1981.

[18] J. A. Goff, J. Chaytor, A. Reed, G. Gawarkiewicz, P. S. Wilson, and D. P. Knobles, "Stratigraphic analysis of a sediment pond within the New England Mud Patch: New constraints from high-resolution chirp acoustic reflection data," *Mar. Geol.*, vol. 412, pp. 81–94, 2019.

[19] J. D. Chaytor, "Measurements of geologic characteristics, geophysical properties, and geoacoustic response of sediments from the New England Mud Patch," *presented at the 2nd Post-Exp. Workshop Seabed Characterization Exp., Appl. Phys. Lab.*, Seattle WA USA, 30–31 May, 2017.

[20] J. Yang and D. Jackson, "Sediment sound speed and bottom model in SBCEXP," *IEEE J. Ocean. Eng.*, to be published.

[21] E. T. Jaynes, *Probability Theory The Logic of Science*, Chapter 10, Cambridge, U.K.: Cambridge Univ. Press, 2003.

[22] E. T. Jaynes, "Information theory and statistical mechanics," *Phys. Rev.*, vol. 106, pp. 620–630, 1957.

[23] E. T. Jaynes, "Information theory and statistical mechanics: II," *Phys. Rev.*, vol. 108, pp. 171–190, 1957.

[24] D. P. Knobles, J. D. Sagers, and R. A. Koch, "Maximum entropy approach for statistical inference in an ocean acoustic waveguide," *J. Acoust. Soc. Amer.*, vol. 131, pp. 1087–1101, 2012.

[25] D. P. Knobles, "Maximum entropy inference of seabed attenuation parameters using ship radiated broadband noise," *J. Acoust. Soc. Amer.*, vol. 138, pp. 3563–3575, 2015.

[26] M. Badiey and I. Jaya, "Shallow water acoustic/geoacoustic experiments at the New Jersey Atlantic Generating Station site," *J. Acoust. Soc. Amer.*, vol. 96, pp. 3593–3604, 1994.

[27] P. H. Dahl *et al.*, "An overview of results from the Asian seas international acoustics experiment in the East China Sea," *IEEE J. Ocean. Eng.*, vol. 29, no. 4, pp. 920–928, Oct. 2004.

[28] G. R. Potty, J. H. Miller, P. H. Dahl, and C. J. Lazauski, "Geoacoustic inversion results from the ASIAEX east China sea experiment," *IEEE J. Ocean. Eng.*, vol. 29, no. 4, pp. 1000–1010, Oct. 2004.

[29] S. D. Rajan, "Waveform inversion for the geoacoustic parameters of the ocean bottom," *J. Acoust. Soc. Amer.*, vol. 91, pp. 3228–3241, 1992.

[30] N. R. Chapman and D. E. Hannay, "Broadband matched field inversion for estimation of geoacoustic properties," in *Shallow Water Acoust.*, R. Zhang and J. Zhou, Eds. Beijing, China: Open Press, 1998, pp. 145–150.

[31] D. P. Knobles, R. A. Koch, L. A. Thompson, and K. C. Focke, "Sound propagation in shallow water and geoacoustic inversion," *J. Acoust. Soc. Amer.*, vol. 113, pp. 205–222, 2003.

[32] A. D. Jones and P. A. Clarke, "Underwater sound received from some defense activities in shallow ocean regions," in *Proc. Annu. Conf. Aust. Acoust. Soc.*, Nov. 3–5, 2004, pp. 467–473.

[33] P. S. Wilson, D. P. Knobles, P. H. Dahl, A. R. McNeese, and M. C. Zey, "Short range signatures of explosive sounds in shallow water used for seabed characterization," *IEEE J. Ocean. Eng.*, to be published.

[34] M. D. Collins, User's Guide for RAM Versions 1.0 and 1.0p, Naval Res. Lab., Washington, DC, USA, Tech. Rep.

[35] I. Goodfellow, Y. Bengio, and A. Courville, *Deep Learning*. Cambridge, MA, USA: MIT Press, 2016, ch. 4. [Online]. Available: http://www.deeplearningbook.org/

[36] S. Kullback and R. A. Leibler, "On information and sufficiency," *Ann. Math. Statist.*, vol. 22, pp. 79–86, 1951.

[37] L. E. Richel, *A Modern Course in Statistical Physics*, 4th ed. Hoboken, NJ, USA: Wiley, 1980.

[38] G. Bilbro and D. E. Van den Bout, "Maximum entropy and learning theory," *Neural Comp.*, vol. 4, pp. 839–853, 1992.

[39] S. Rutherford and K. E. Hawker, "Effects of density gradients on bottom reflection loss for a class of marine sediments," *J. Acoust. Soc. Amer.*, vol. 63, pp. 750–757, 1978.

[40] M. J. Buckhingham, "Compressional and shear wave properties of marine sediments: Comparisons between theory and data," *J. Acoust. Soc. Amer.*, vol. 117, pp. 137–152, 2005.

[41] E. L. Hamilton, "Sound velocity gradients in marine sediments," *J. Acoust. Soc Amer.*, vol. 65, pp. 909–922, 1979.

[42] H. E. Morris, "Bottom-reflection-loss model with a velocity gradient," *J. Acoust. Soc. Amer.*, vol. 48, pp. 1198–1202, 1970.

[43] J. X Zhou, X. Z. Zhang, and P. H. Rogers, "Effect of frequency dependence of sea-bottom attenuation on the optimum frequency for acoustic propagation in shallow water," *J. Acoust. Soc. Amer.*, vol. 82, pp. 287–292, 1987.

[44] R. B. Evans and W. M. Carey, "Frequency dependence of sediment attenuation in two-frequency shallow-water acoustic experimental data sets," *IEEE J. Ocean. Eng.*, vol. 23, no. 4, pp. 439–447, Oct. 1998.

[45] S. K. Mitchell and K. C. Focke, "The role of sea-bottom attenuation profile in shallow-water acoustic propagation," *J. Acoust. Soc. Amer.*, vol. 73, pp. 465–473, 1983.

[46] A. C. Kibblewhite, "Attenuation of sound in marine sediments: A review with emphasis on new low-frequency data," *J. Acoust. Soc. Amer.*, vol. 86, pp. 716–738, 1989.

[47] J. X Zhou, X. Z. Zhang, P. Rogers, and J. Jarzynski, "Geoacoustic parameters in a stratified sea bottom from shallow water acoustic propagation," *J. Acoust. Soc. Amer.*, vol. 82, pp. 2068–2074, 1987.

[48] D. P. Knobles, T. W. Yudichak, R. A. Koch, P. G. Cable, J. H. Miller, and G. Potty, "Inferences of seabed attenuation from distributed acoustic measurements in the East China Sea," *IEEE J. Ocean. Eng.*, vol. 31, no. 1, pp. 129–144, Jan. 2006.

[49] J. D. Holmes, W. M. Carey, S. M. Dediu, and W. L. Siegmann, "Nonlinear frequency-dependent attenuation in sandy sediments," *J. Acoust. Soc. Amer.*, vol. 121, pp. EL218–EL222, 2007.

[50] D. P. Knobles, P. S. Wilson, J. A. Goff, and S. E. Cho, "A seabed acoustics experiment on a sand ridge on the New Jersey continental shelf," *J. Acoust. Soc. Amer.*, vol. 124, pp. EL151–EL156, 2008.

[51] J. X Zhou, X. Z. Zhang, and D. P. Knobles, "Effective geo-acoustic model for sandy seabottoms in shallow water," *J. Acoust. Soc. Amer.*, vol. 125, pp. 2647–2666, 2009.

[52] G. Potty, J. H. Miller, J. F. Lynch, A. Newhall, and P. S. Wilson, "Compressional wave speed and attenuation inversions using combustive sound source signals," *IEEE J. Ocean. Eng.*, to be published.

[53] L. Wan, J. X Zhou, and P. H. Rogers, "Low-frequency sound speed and attenuation in sandy seabottom from long-range broadband acoustic measurements," *J. Acoust. Soc. Amer.*, vol. 128, pp. 578–589, 2010.

[54] L. Wan, M. Badiey, and D. P. Knobles, "Geoacoustic inversion using low frequency broadband acoustic measurements from L-shaped arrays in the Shallow Water 2006 experiment," *J. Acoust. Soc. Amer.*, vol. 140, pp. 2358–2373, 2016.

[55] L. Wan, M. Badiey, D. P. Knobles, and P. S. Wilson, "The Airy phase of explosive sounds in shallow water," *J. Acoust. Soc. Amer.*, vol. 143, pp. EL199–EL205, 2018.

[56] M. J. Buckingham, "Compressional and shear wave properties of marine sediments: Comparisons between theory and data," *J. Acoust. Soc. Amer.*, vol. 117, pp. 137–152, 2005.

[57] M. J. Buckingham, "On pore-fluid viscosity and the wave properties of saturated granular materials including marine sediments," *J. Acoust. Soc. Amer.*, vol. 122, pp. 1486–1501, 2007.

[58] A. Mallock, "The damping of sound by frothy liquids," *Proc. Roy. Soc. London A*, vol. 84, no. 572, pp. 391–395, 1910.

[59] A. B. Wood, *A Textbook of Sound*, 1st ed. New York, NY, USA: MacMillan, 1930.

David P. Knobles received the Ph.D. degree in nuclear theory in 1989 from the University of Texas at Austin, Austin, TX, USA.

From 1989 to 1992, he did a Postdoctoral Fellowship in nuclear physics with the University of Texas at Austin. He was a Research Scientist with The Applied Research Laboratories, The University of Texas at Austin, from 1980 to 1985 and 1992 to 2016. He is currently the owner of Knobles Scientific and Analysis, a private business that specializes in defense and environmental applications. He has been a Principle Investigator with the Ocean Acoustics Program, the Office of Naval Research, since 2002. He has taught graduate courses at UT-Austin in methods of mathematical physics and ocean acoustics. He is currently serving as a Co-Chief Scientist for the ONR Seabed Characterization Experiment. His research interests include theoretical physics, remote sensing, cosmology, and bioacoustics.

Dr. Knobles is a Fellow of the Acoustical Society of America.

Preston S. Wilson received the B.S.M.E. and M.S.M.E. degrees in mechanical engineering from The University of Texas at Austin, Austin, TX, USA, in 1990 and 1994, respectively, and the Ph.D. degree in mechanical engineering from Boston University, Boston, MA, USA, in 2001.

He is currently a Professor and Raymond F. Dawson Centennial Fellow in engineering with the University of Texas at Austin, with joint appointments with the Department of Mechanical Engineering and Applied Research Laboratories (ARL:UT). He was a Research Engineer with ARL:UT from 1993 to 1997, served as a Postdoctoral Fellow with Boston University from 2001 to 2003, and has been a Faculty Member with UT Austin since 2003. His work has been reported in more than 360 peer-reviewed papers, conference proceedings, technical reports, and published presentation abstracts. He holds six US patents, and is a Co-Founder of AdBm, Inc., operating in the underwater noise mitigation arena. He is currently serving as a Co-Chief Scientist for the ONR Seabed Characterization Experiment. His research areas are broadly focused on physical acoustics, underwater acoustics, engineering acoustics, and bioacoustics, with specific areas of interest in sound propagation in shallow water, in water-saturated sediments, bubbly liquid, and multiphase material.

Dr. Wilson was the recipient of the A. B. Wood Medal from the Institute of Acoustics U.K., is a Fellow of the Acoustical Society of America (ASA), the Past Chair of the Committee for Education in Acoustics of the ASA, a current member of the Executive Council of the ASA, and an Associate Editor of the *Journal of the Acoustical Society of America*.

John A. Goff received the Sc.B. degree in geophysics math from Brown University, Providence, RI, USA, in 1985, and the Ph.D. degree in oceanography from the MIT/Woods Hole Oceanographic Institution Joint Program, Woods Hole, MA, USA, in 1990.

After two years of Postdoctoral work with WHOI, he took a position as a Research Associate with the University of Texas Institute for Geophysics in 1993. He was promoted to Research Scientist in 1999, and then Senior Research Scientist in 2004. His work has resulted in more than 100 peer-review publications as author or coauthor. His research employs swath sonar mapping and high-resolution reflectivity imaging to investigate morphology of the seafloor, its pattern of acoustic reflectivity, and shallow stratigraphy. His research interests are focused on sedimentary processes and structures in coastal and continental shelf settings, with recent efforts dedicated to understanding the impacts of hurricanes, tsunamis, and glaciers on the near-shore sedimentary processes.

Lin Wan received the double B.S. degrees in mechanical engineering and electrical engineering and the M.S. degree in ocean acoustics from Shanghai Jiao Tong University, Shanghai, China, in 2000 and 2003. He received the M.S. degree in industrial engineering and the Ph.D. degree in mechanical engineering from the Georgia Institute of Technology, Atlanta, GA, USA, in 2008 and 2010, respectively.

During his Ph.D. study, he was a U.S. Office of Naval Research (ONR) Graduate Traineeship Awardee supported by the special research award from the Ocean Acoustics program. Then, he worked as a Postdoctoral Fellow with the School of Mechanical Engineering, Georgia Tech. After his Postdoctoral Research with Georgia Tech, he joined the Ocean Acoustics Laboratory, University of Delaware, Newark, DE, USA, where he is currently a Research Associate in Electrical and Computer Engineering Department. He has been conducting experimental and theoretical research in ocean acoustics, acoustical oceanography, and acoustic signal processing. He is the Principal Investigator of an ONR grant to study the geoacoustic properties in muddy sediments using broadband acoustic signals. His research interests include geoacoustic inversion and internal wave effects on three-dimensional sound propagation in shallow water.

Dr. Wan is a member of the Acoustical Society of America.
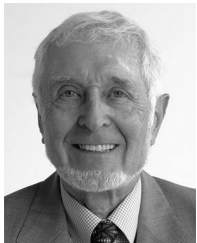
Michael J. Buckingham received the B.Sc.(Hons.) degree in physics and the Ph.D. degree in solid-state physics from the University of Reading, Reading, U.K., in 1967 and 1971, respectively .

He is currently a Distinguished Professor of Ocean Acoustics with the Marine Physical Laboratory, Scripps Institution of Oceanography, University of California, San Diego, CA, USA. He has been a Visiting Professor with the Institute of Sound and Vibration Research, University of Southampton, Southampton, U.K., with the National Key Laboratory of Science and Technology on Sonar, China, and with the Department of Ocean Engineering, M.I.T. Before joining Scripps, he was an Individual Merit Senior Principal Scientific Officer with the Royal Aerospace Establishment (RAE), Farnborough, U.K. While at RAE, he was an Exchange Scientist, attached to the British Embassy, with the Naval Research Laboratory, Washington, D.C., USA. He also served as the U.K. National Representative on the Scientific Committee of the Marine Science and Technology (MAST) Programme, Commission of European Communities, Brussels, Belgium. He is a Chartered Engineer in U.K. Buckingham has published a book on *Noise in Electronic Devices and Systems* (Horwood, 1985), and he is a Co-Editor of Sea Surface Sound '94, Proceedings of the III International Meeting on Natural Physical Processes Related to Sea Surface Sound. His research has been reported in more than 250 papers, articles, and reports in the scientific literature.

Dr. Buckingham was honored to serve as the Vice President of the Acoustical Society of America. Along with several other awards for his research on underwater acoustics, he was the recipient of the A. B. Wood Medal from the Institute of Acoustics, U.K., and the Pioneers of Underwater Acoustics Medal from the Acoustical Society of America. He is a Fellow of the Acoustical Society of America, the Institute of Acoustics (U.K.), and the Institution of Engineering and Technology (U.K.). He is currently an Editor-in-Chief for the *Journal of Computational Acoustics* and he was the Editor of Reviews in Physical Acoustics for the *Journal of Sound and Vibration*.

Jason D. Chaytor received the Graduate degree from the Queensland University of Technology, Brisbane, Qld., Australia, in 2000, with a first-class honours degree in geology, and the Ph.D. degree in geological oceanography from Oregon State University, Corvallis, OR, USA, in 2006.

He is currently a Research Geologist with the U.S. Geological Survey, USGS Woods Hole Coastal and Marine Science Center. He was a Postdoctoral Scholar with Woods Hole Oceanographic Institution between 2006 and 2009. He conducts research on issues related to marine geohazards including submarine landslides, tsunamis, earthquakes, and plate tectonics and shallow- and deep-water sedimentary processes on Atlantic, Gulf of Mexico, and Pacific margins of the U.S. and in the northeast Caribbean. He is currently the Principle Scientist for the USGS Woods Hole Coastal and Marine Science Center Sediments Laboratory.

Mohsen Badiey received the Ph.D. degree in applied marine physics and ocean engineering from Rosenstiel School of Marine and Atmospheric Science, University of Miami, Coral Gables, FL, USA, in 1988.

From 1988 to 1990, he was a Postdoctoral Fellow with the Port and Harbor Research Institute, Ministry of Transport in Japan. After his Postdoctoral research, he became a Faculty Member with the University of Delaware, Newark, DE, USA, where he is currently a Professor. From 1992 to1995, he was a Program Director and Scientific Officer with the Office of Naval Research where he served as the Team Leader to formulate long-term naval research in the field of Acoustical Oceanography. His research interests are physics of sound and vibration, shallow water acoustics and oceanography, underwater acoustic communications, seabed acoustics, and geophysics.

Dr. Badiey is a Fellow of the Acoustical Society of America.